Resolution of the anomalous fission fragment anisotropies for the $^{16}O + ^{208}Pb$ reaction

C.R. Morton, D.J. Hinde, J.R. Leigh, J.P. Lestone,* M. Dasgupta, J.C. Mein, J.O. Newton, and H. Timmers
Department of Nuclear Physics, Research School of Physical Sciences and Engineering, Australian National University, Canberra, ACT 0200, Australia
(Received 27 March 1995)

Fission and evaporation residue cross sections and fission fragment angular distributions have been measured for the reaction $^{16}O + ^{208}Pb$ in small energy steps spanning the barrier region. Fission fragment anisotropies have been calculated using the transition state model, making use of spin distributions more accurately determined from the new cross-section data, and a more realistic calculation of the nuclear temperatures at the saddle-point. Comparison of these calculations with the new experimental anisotropies show no evidence for anomalously large fission fragment anisotropies at beam energies below the average fusion barrier. Thus, the standard models of fusion and fission are able to describe the new data.

PACS number(s): 25.70.Jj

I. INTRODUCTION

The angular distribution of fission fragments can be characterized by its anisotropy A, defined as the ratio of the yield at 180° (or 0°) to that at 90°. In the transition state model [1], the fission fragment anisotropy can be approximately written as

$$A = W(180°)/W(90°) \approx 1 + \frac{\langle J^2\rangle \hbar^2}{4(T\mathcal{J}_{\rm eff})}, \qquad (1)$$

where $\mathcal{J}_{\rm eff}$ is the effective moment of inertia of the saddle-point (transition state) configuration, T is the temperature at the saddle-point, and J is the total angular momentum of the fissioning system. In heavy-ion-induced fission, if it is assumed that complete fusion occurs, then for a spin-zero target and projectile, J can be identified with the orbital angular momentum l of the projectile, corrected for the effect of particle emission.

If two of the variables in Eq. (1) are known, the third quantity may be extracted from the measured anisotropy. For fissile systems, this procedure has been used to obtain information on the mean-square angular momentum $\langle l^2\rangle$ to test theoretical models of fusion. However, the results from this method have not been in agreement with the predictions of fusion models, particularly at energies below the average barrier, where the measured anisotropies (or deduced $\langle l^2\rangle$ values) have been considerably larger than expected [2]. This is in contrast to the situation for other techniques determining $\langle l\rangle$, where there has been general agreement between theory and the data, for all but the most mass-symmetric systems [3–5].

A number of reasons for the failure of the fission fragment angular distribution technique has been put forward, including the effect of fission following transfer reactions [6,7] and contributions from quasifission [8–10]. For fissile systems with projectile masses $A \geq 24$, it is accepted [8] that quasifission becomes a significant reaction mechanism. Quasifission is thought [11] to correspond to formation of a dinuclear system which never becomes as compact as the unconditional saddle-point configuration. Experimentally, a large anisotropy, a wide mass distribution, and a correlation of mean fragment mass with angle are observed [11]. The anisotropy is the most easily measured, and it could be argued that this is the most sensitive observable for detecting quasifission, provided that the anisotropy for fusion-fission can be reliably calculated.

Whether this can be done is brought into question by the measured anisotropies for the $^{16}O + ^{208}Pb$ reaction. For this fusion reaction, standard barrier passing models are expected to be applicable. Furthermore, on the basis of the anisotropy at energies above the average fusion barrier, there was no evidence for quasifission [12]. Nevertheless, at energies below the average barrier, measured anisotropies exceeded those calculated by a significant amount [9]. Since the temperature of the system at the saddle-point is an important quantity in the calculation, a measurement was made of the pre-scission neutron multiplicity [13] and, with the assumption of exclusive pre-saddle emission, the mean excitation energy removed by evaporation before the system crossed the saddle-point was determined. Although the lower saddle-point temperature resulted in a larger calculated anisotropy, an anomaly remained at energies below the average barrier (see Fig. 7 of Ref. [13]). Thus, it could be concluded that either the fusion models were wrong, or the theory of fission fragment angular distributions was in error or inapplicable. A third possibility, though thought unlikely, was that there may be a significant quasifission yield only at energies below the average fusion barrier. Recently [14], this has been shown to be the case for the $^{16}O + ^{238}U$ reaction, where the anisotropies were found to be correlated with the orientation of the deformed target nuclei.

It has been proposed by several authors [15] that a model of fusion which successfully reproduces the energy

*Present address: Nuclear Physics Laboratory, University of Washington, Seattle, WA 98195.

dependence of the fusion cross section should also correctly predict the angular momentum distribution. Recent developments in the precise measurements of fusion excitation functions [16–18], and their interpretation in terms of the mean angular momentum [19], have led to the conclusion that details of the angular momentum distributions can be extracted from a precision measurement of the fusion excitation function. In the case of the $^{16}O + ^{208}Pb$ reaction, the evaporation residue (ER) component of the fusion excitation function has proved difficult to determine accurately. Two previous measurements of the ER cross sections for this system were in conflict by up to a factor of four [20,21]. Recently, Brinkmann *et al.* [22] have remeasured the ER excitation function, obtaining cross sections that are larger still, with their maximum value around four times the maximum of Ref. [21]. It will be shown that discrepancies in the ER cross sections of the above magnitude are very significant when calculating theoretical fission fragment anisotropies. In order to more accurately define the excitation function for the $^{16}O + ^{208}Pb$ reaction, both the evaporation residue and fission cross sections have been remeasured in detail, the latter measurement also yielding the fission fragment anisotropies.

In the next section, a description is given of how each component of the fusion cross section was measured. In Sec. III, the excitation function for each component is presented. In Sec. IV, the experimental anisotropy is compared with transition state model calculations. The experimental anisotropies from this work are found to be in agreement with these improved theoretical calculations.

II. EXPERIMENTAL PROCEDURE

The experiments were performed with a pulsed beam of ^{16}O from the 14UD tandem accelerator at the Australian National University. The beam energy of the projectiles was defined to better than 0.05 MeV [18]. Fission excitation functions were measured using ^{208}PbS targets of 350 and 23 $\mu g\,cm^{-2}$, deposited on ≈ 10 $\mu g\,cm^{-2}$ C backings. The evaporation residues were measured in a separate experiment with the 350 $\mu g\,cm^{-2}$ target.

A. Fission fragment angular distributions

Fission fragments were detected in a large-area multiwire proportional counter (MWPC), position sensitive in two dimensions. The MWPC consists of a plane of vertical (x-plane) and horizontal (y-plane) wires each located 3 mm either side of a central foil. The distance between each wire is 1 mm, and the signals from these wires passed through a delay line with a 1 ns delay between each wire. The detector was placed 180 mm from the target, giving an angular coverage of $95° \leq \theta_{lab} \leq 170°$ in the backward hemisphere. The active area subtended a solid angle of 0.68π sr, which permitted very efficient data collection, with high statistical precision in a short period of time. The central foil provided an energy loss (ΔE) signal and time-of-flight (TOF) information with respect to the pulsed beam (1 ns width and 106.3 ns separation). This enabled identification of the fission fragments. Figure 1 shows ΔE plotted as a function of TOF for slices of width $\Delta\theta_{lab} = 5°$, at the angles given, for a beam energy close to that of the average fusion barrier. The fission fragments are well separated from the elastically scattered events at all angles, confirming that this identification technique allowed accurate determination of the fission fragment angular distributions.

Two Si surface-barrier detectors, positioned at $\pm 17°$ relative to the beam axis, were used to monitor the Rutherford scattering yield. Each event at position (x, y) on the active area of the detector was transformed to give the scattering angle θ_{lab} and the azimuthal angle ϕ_{lab} with respect to the beam axis. For a constant cut of $\Delta\phi_{lab} = 57°$, events were put into bins of $\Delta\theta_{lab} = 5°$. The differential cross sections $d\sigma_{fis}/d\Omega$ per bin were obtained by calibrating each 5° bin using Rutherford scattering of ^{28}Si projectiles. These cross sections were then transformed to the center-of-mass reference frame assuming symmetric fission, with total kinetic energies from the Viola systematics [23]. Figure 2 shows an example of the differential fission cross sections as a function of $\theta_{c.m.}$ for the beam energies indicated. The error bars on $d\sigma_{fis}/d\Omega$ in Fig. 2 result from statistical uncertainties only.

The calibration of the x and y position spectra was carried out assuming a linear relationship between the

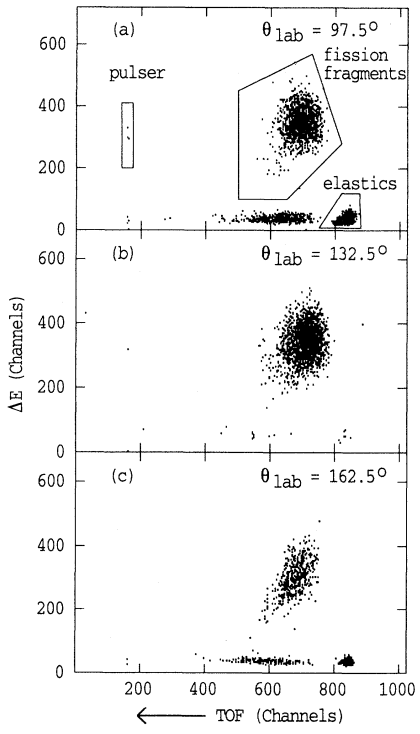

FIG. 1. A plot of the energy loss signal from the central foil of the detector as a function of the time of flight for $E_{lab} = 79.5$ MeV for three different angles slices in the (a) forward, (b) middle, and (c) backward angle regions, each of 5° width.

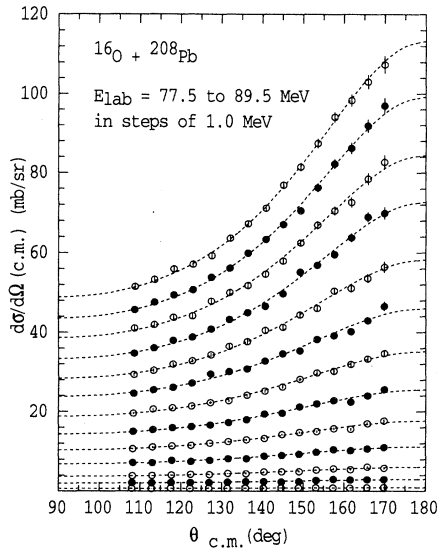

FIG. 2. The experimental fission fragment angular distributions as a function of the center-of-mass scattering angle for one measurement of the excitation function. The dashed lines are fits to the data using the transition state model. The error bars on the data points indicate statistical uncertainties.

time difference from the delay line and the position of each event. The elastic scattering calibration measurement showed that for 5° bins, this relationship was true to within ±5%, and allowed corrections for nonlinearities to be made. Any difference between the corrections determined during the calibration run and those applicable during the fission measurements will cause small distortions in the measured fission fragment angular distribution by redistributing the events. However, this has a negligible effect on the total fission cross section.

To obtain the total fission cross section and the fission fragment anisotropy it was necessary to extrapolate to $\theta_{\mathrm{c.m.}}$ beyond the detector's angular coverage. This was accomplished by fitting the angular distribution using the transition state model procedure of Back *et al.* [12], assuming that the angular distribution in the extrapolated regions can be so described. The dashed lines in Fig. 2 show the quality of this fit, which gave confidence that the angular range covered in this experiment allowed the anisotropy to be well defined.

B. The evaporation residue measurement

The evaporation residue excitation function was determined by detecting the α activity from the decay of the evaporation residues and their daughters. The recoiling evaporation residues were stopped in an Al catcher foil of $\approx$ 800 μg cm^{-2}, positioned immediately behind the target. Their subsequent α decays were detected using an annular Si surface barrier detector which viewed the target and catcher foil directly. The detector was placed at a mean angle of 164° to the beam direction. Again, two monitor detectors were used to normalize the measured yield to obtain the ER cross sections. The relative solid angle of the annular counter was determined *in situ* using Rutherford scattering. For the α-decay measurement, the beam was pulsed (3.12 μs on, 21.3 μs off), and the energy and arrival time of the α particles were collected for 19.5 μs during the beam off period. Each evaporation channel is characterized by a decay chain whose α energies and half-lives are well known [24]. The α lines in this chain have fixed, beam energy independent relative intensities, which were calculated from the known branching ratios, the half-lives, and the experimental counting period. At each bombarding energy, the contributions of the possible evaporation channels to the measured α spectrum were obtained using a peak fitting routine that gave the cross sections for the individual evaporation channels and, hence, the total ER cross section. The α spectrum obtained for a bombarding energy of E_{lab} = 84.0 MeV is shown in Fig. 3. The α spectrum was fitted for energies above 7.8 MeV because of the presence of long-lived ($t_{1/2} > 0.5$ s) contaminant activity around 7.4 MeV. This threshold energy had little effect since almost all of the α-activity from the ERs is above 7.8 MeV. The ER excitation functions for the evaporation channels are shown in Fig. 4(a). For clarity, the sums of the αxn and pxn channels are given. The sums of all the evaporation channels using this fitting procedure are shown in Fig. 4(b).

Because of the complex nature of the α spectra and the multiple lines associated with each evaporation channel, the fitting procedure generated unrealistic fluctuations in some of the weaker channels, as shown in Fig. 4. This caused a small scatter in the ER cross sections. It was possible to reduce the dependence of the ER cross sections on the fitting procedure, by making use of the mean decay α multiplicities $\overline{M}_{\alpha}(E)$. They were evaluated at each energy using

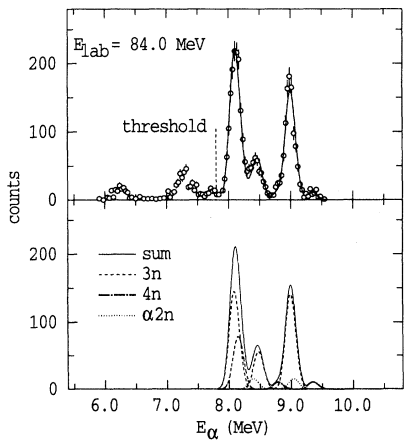

FIG. 3. The measured α spectrum obtained at an energy E_{lab} = 84.0 MeV. The solid line is the peak fit to the data, fitted for α energies above the threshold energy of 7.8 MeV. The lower panel shows the breakdown of this fit into its constitute channels. The $3n$ channel dominates at this energy.

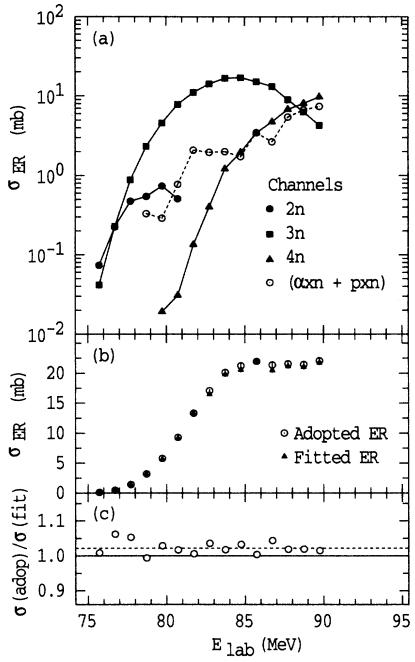

FIG. 4. (a) The ER cross sections for each evaporation channel obtained by fitting the α-particle energy spectra. The αxn and pxn channels have been summed for clarity (open circles). (b) The ER excitation functions from the two analyses. The sum of each evaporation channel as determined from the peak fitting analysis (triangles), and the smoothed excitation function obtained using the α-decay multiplicities (open circles). The latter was adopted in this work. (c) The ratio of the adopted to the peak fitted excitation functions. This shows that the fitting procedure accounts for all the evaporation channels down to the $\approx 2\%$ level (dashed line).

$$\overline{M}_\alpha(E) = \sum_i f_i(E) M_\alpha^i, \tag{2}$$

where $f_i(E)$ is the fraction of the ER cross section and M_α^i are the decay α-multiplicities in channel i. Since the excitation functions of each channel vary slowly and smoothly, typically over an energy range of ≈ 10 MeV, $\overline{M}_\alpha(E)$ cannot change rapidly. Indeed, the extracted values of $\overline{M}_\alpha(E)$ vary by only 30% over an energy range of 15 MeV. Smoothing of the $\overline{M}_\alpha(E)$ over ± 2 MeV in order to minimize scatter is then reasonable. A second ER excitation function was then generated using the total α yield above 7.8 MeV, instead of the fitted yield used previously, divided by the smoothed $\overline{M}_\alpha(E)$. This second excitation function is shown by the open circles in Fig. 4(b). The consistency between the two approaches is illustrated in Fig. 4(c), where the ratio of the two excitation functions is plotted. The smoothed cross sections were typically 2% larger than those obtained from the fitting procedure, perhaps reflecting the effects of weak evaporation channels rejected in the fitting process or of imperfect matching of the peak shapes. The smoothed excitation function was the one adopted in this work.

III. RESULTS

The fission cross sections for the $^{16}O + ^{208}Pb$ reaction were obtained by integrating the fitted angular distributions. The results are shown in Fig. 5(a), together with previous measurements for this system [25,12,20,9]. Good agreement is observed within the experimental uncertainty, except for the data of Murakami *et al.* [9], where an energy shift of -0.7 MeV was required to obtain agreement with the other data sets.

The ER cross sections from the α-decay measurement are shown in Fig. 5(b) along with the recent data of Brinkmann *et al.* [22]. Although not all the data points are in agreement, the relatively good agreement between these two data sets confirms that the previously measured cross sections [20,21] were too low. The reasons why these two measurements [20,21] disagree are not clear. The reasonable consistency in σ_{ER} from Brinkmann *et al.* [22] and the results of this work give confidence that these cross sections are now known to a satisfactory accuracy.

The total fusion cross section was obtained by summing the fission and evaporation residue cross sections of Fig. 5 at each energy. At energies where the ER cross section was not available, an interpolated ER value was

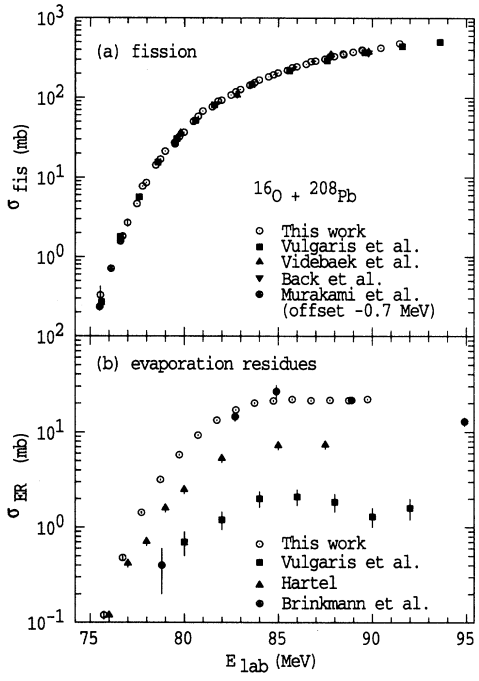

FIG. 5. (a) The fission cross sections from this work (open circles) as a function of E_{lab}. Also shown are the data of Vulgaris *et al.* [20] (solid squares), Videbæk *et al.* [25] (solid triangles), Back *et al.* [12] (inverted solid triangle), and Murakami *et al.* [9] (solid circles). The data of Murakami *et al.* has been offset by -0.7 MeV. (b) The experimental evaporation residue cross sections from this work (open circles) and the earlier data of Vulgaris *et al.* [20] (solid squares), Hartel [21] (solid triangles), and Brinkmann *et al.* [22] (solid circles).

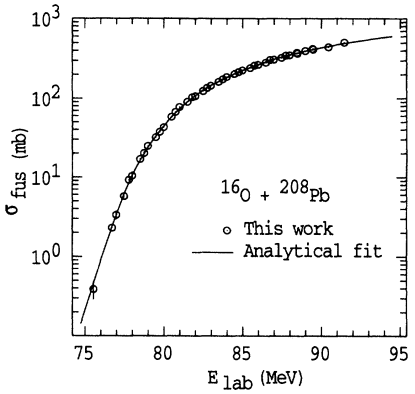

FIG. 6. The experimental fusion excitation function (open circles) obtained from summing the ER and fission excitation functions. The solid line represents the analytical eigenbarrier fit to the cross sections.

used. This procedure gave a negligible additional uncertainty in the fusion cross sections, since the ER cross sections are well-defined, and represent a small fraction of the fusion cross section, which decreases with increasing energy. The fusion excitation function is shown in Fig. 6.

The distribution of fusion barriers [26] was obtained from the fusion excitation function by evaluating the point difference formula of Ref. [16] using an energy step of 1.86 MeV [see Fig. 7(a)]. Conservatively, it was assumed that the uncertainties in the fusion cross sections were ±1% or, at the lowest beam energies, as given by the counting statistics, whichever was larger.

The experimental fission fragment anisotropies are shown by the open circles in Fig. 7(b), as a function of $E_{\rm c.m.}$. The error bars on the anisotropies are from the statistical uncertainties in the angular distribution of the fission fragments. Comparison with Fig. 7(a) shows that the measured anisotropies decrease smoothly and monotonically as the beam energy falls through the barrier region. There is no evidence for any feature in the anisotropies. This is in contrast to the situation for the ^{16}O + ^{238}U reaction [14]. The measurements of the angular distributions were carried out in three separate experiments, each with its own calibration measurement. The data points appear to have a small additional scatter, which was attributed to slight changes in the calibration of the 5° bins. As shown in Fig. 7(b), the effect is not much larger than would be expected simply on the basis of the statistical error bars shown, and an additional ±3% uncertainty would encompass this scatter. The solid data points are from the previous work of Back *et al.* [12], Vulgaris *et al.* [20], and Murakami *et al.* [9]. The overall agreement is reasonable. However, the previously measured anisotropies at the energies $E_{\rm c.m.} = 71$ and 72 MeV, below the average barrier, are larger than the present measurements.

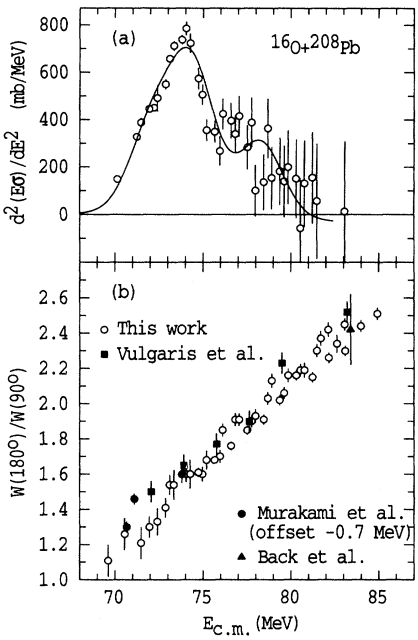

FIG. 7. (a) The experimental distribution of fusion barriers for the ^{16}O + ^{208}Pb reaction (open circles). The solid line is the empirical model fit to the fusion data. (b) The experimental fission fragment anisotropies (open circles) as a function of $E_{\rm c.m.}$. The solid points are the results of previous measurements. The data of Murakami *et al.* [9] have been offset by −0.7 MeV, as in Fig. 5(a).

IV. COMPARISON OF THE EXPERIMENTAL ANISOTROPIES WITH THE TRANSITION STATE MODEL

The standard model for interpretation of fission fragment angular distributions, the transition state model (TSM), requires knowledge of the total angular momentum J of the fissioning nucleus, the temperature T of the fissioning nuclear system at its transition state, taken to be the saddle-point, and the effective moment of inertia at the saddle-point $\mathcal{J}_{\rm eff}$. It is important to determine these quantities to the best possible accuracy in order to test the agreement between the experiment and the calculations from the transition state model. In this section, a description is given of how each of these quantities was determined. Then, comparisons between the experimental data and the theory are made in terms of the reduced anisotropy $(A-1)$, which is approximately proportional to $\langle J^2\rangle/(T\mathcal{J}_{\rm eff})$. It should be emphasized that all calculations of the anisotropy were carried out using the rigorous expressions detailed in Back *et al.* [12], not the approximate expression given in Eq. (1).

A. Effective moment of inertia at the saddle-point

To determine the spin-dependent moments of inertia perpendicular and parallel to the symmetry axis, a simple parametrization [27] of the rotating finite-range model

(RFRM) was used. This provides a fast way of approximating a full RFRM calculation, and is adequate for the heavy system studied here. The value of the effective moment of inertia for $l = 0$ at the saddle-point was $\mathcal{J}_{\text{eff}} = 4600$ u fm^2. This value is $\approx 3\%$ larger than the RFRM value. Since the reduced anisotropy is approximately proportional to $1/\mathcal{J}_{\text{eff}}$, use of the RFRM value would scale the reduced anisotropy in an approximately linear way, resulting in an equivalent increase in $(A-1)$. The true value of the effective moment of inertia is one of the remaining uncertainties in these TSM calculations.

B. Temperature at the saddle-point

Neutron emission in competition with fission before passage over the saddle reduces the temperature of the fissioning system at its saddle-point. However, neutron emission during the saddle-to-scission transition does not alter the saddle-point temperature, and so has no bearing on the TSM calculation of the anisotropies. It was shown in Ref. [13] that for energies up to $E_{\text{c.m.}} \approx 92$ MeV, most of the measured pre-scission neutrons should be emitted before the saddle-point is reached, and that the lower the energy, the more reliable the assumption. It was demonstrated that the calculated anisotropies were in better agreement with the data at low energies when the loss of excitation energy due to neutron emission was accounted for, but deviated from experimental values at higher energies ($E_{\text{c.m.}} \gtrsim 92$ MeV). A recent calculation [28] has shown that for these higher energies, an appreciable number of neutrons may be emitted during the saddle-to-scission transition time, thus putting the theory back in better agreement with the data in the high-energy region. However, an anomaly still persists at the lower energies.

An approximation of the previous analysis of Rossner *et al.* [13] was that the temperature at the saddle-point was calculated for the *mean* value of the excitation energy of the fissioning systems. This approach results in a smaller anisotropy compared to a more realistic calculation which evaluates the anisotropy for a *distribution* of excitation energies. The approximation becomes worse as the spread in the range of excitation energies increases. In this work, the compound nucleus decay was modeled with the Monte Carlo evaporation code JOANNE [29], which gave a distribution of excitation energies, allowing the temperature at the saddle-point to be determined on an event-by-event basis. With this approach, all correlations of the excitation energy, $\mathcal{J}_{\text{eff}}(l)$, and l are retained.

The Monte Carlo evaporation code modeled the decay of the compound nuclei in order to determine the distribution of events into the competing fission and ER modes. The pre-scission neutron multiplicity data of Ref. [13] and the evaporation residue cross sections from this work were fitted with the code JOANNE. This was done by varying the level density parameter at the saddle-point a_f and the Sierk fission barrier scaling factor k_f. The level density parameter at the equilibrium deformation, a_n, was taken to be $a_n = A/8.8$ MeV^{-1}. The temperature at the saddle-point for a nucleus with an excitation energy E^* was obtained from

$$T_J^2 = [E^* - k_f B_f(J) - E_{\text{rot}}(J) - E_n(J)]/a_f, \quad (3)$$

where $B_f(J)$ is the Sierk fission barrier [30], $E_{\text{rot}}(J)$ is the rotational energy of the equilibrium configuration from the RFRM, and $E_n(J)$ is the reduction in excitation energy due to the evaporation of neutrons. The excitation energies were calculated using liquid-drop masses for the compound nuclei. Fits to the pre-scission neutron multiplicities and the ER excitation functions were obtained for average values of $a_f/a_n = 0.90$ and $k_f = 0.88$. Because of the significant contribution of fission from very low excitation energies, which is not well modeled in this code since shell effects are not included, the parameters cited above can only be considered as fit parameters which result in the correct energy loss before fission and the correct survival probability. The effect on the distribution of excitation energies due to variation of these statistical model parameters was also examined. For example, the pre-scission neutron multiplicities and the ER cross sections were fitted with $a_f/a_n = 1.00$ and $k_f = 0.70$, after hindering the fission process with the introduction of a constant Kramers scaling factor [31]. Because of the uncertainty in the excitation energy due to shell effects, other calculations were performed with different reaction Q values. The anisotropies from these calculations never varied by more than 3%, provided that the pre-scission neutron multiplicities and the ER cross sections were fitted. This indicates a reasonable insensitivity of the anisotropy to different starting assumptions, as long as the relevant experimental quantities are reproduced.

C. Spin distributions of the fissioning nuclei

The compound nucleus spin distributions were determined from the fusion excitation function, assuming that a model which fits the fusion cross sections gives the spin distributions [15,19]. A fit to the experimental fusion cross sections was performed using an "analytical eigenbarrier" approach. Here, the fusion cross section is given by

$$\sigma(E) = \sum_{\beta} w_\beta \sigma(E, B_\beta), \quad (4)$$

where $\sigma(E, B_\beta)$ is the cross section for each eigenbarrier with height B_β, and w_β is the weight for each eigenbarrier in eigenchannel β. A fit to the high-energy data, using the Wong form of the fusion cross section, as described in Ref. [19], determined the radius and curvature of the s wave barrier. The average barrier height was $B_0 = 74.6$ MeV. Then, a χ^2 fit to the experimental cross sections over the entire energy range determined the optimum number of barriers and their weights. The best fit was found with three barriers, giving rise to the distribution of barriers shown by the solid line in Fig. 7(a) and the excitation function shown by the solid line in Fig. 6. An ambiguity in this approach is in the choice of the radius of the eigenbarriers. For this calculation of the spin distributions, all barrier radii were set to the av-

erage barrier radius. The effect on the spin distributions of using a radius that depends on each eigenbarrier, following Eq. (7) in Ref. [19], instead of the average radius, was investigated. The difference between the calculated anisotropies in these two approaches was not significant.

The spin distributions of the fissioning nuclei are slightly different to those of the compound nuclei because of the pre-saddle particle emission. This effect was taken into account in the JOANNE calculation which corrected the above spin distributions. It was assumed that all the compound nuclei are formed in complete fusion reactions.

In the comparison of the mean-square angular momentum obtained from the anisotropies and those values from various fusion models presented in Ref. [9], there was an ambiguity in the evaporation residue cross sections. The measurements of $\sigma_{\rm ER}$ by Hartel [21] were up to four times larger than those of Vulgaris *et al.* [20]. Similarly, the analysis of Ref. [13] depended upon knowledge of the evaporation residue survival probabilities, for two reasons. The ER cross sections have an influence on the spin distributions for fusion and also on the saddle-point temperature of the fissioning nuclei. As shown in the subsection below, the latter has the most significant effect on the anisotropy.

D. Comparison with the experimental anisotropies

The evaporation code JOANNE was used to calculate the distribution of saddle-point temperatures and spins of the fissioning systems, after the evaporation of neutrons. Fission events were put into bins of J and T with width $1\hbar$ and 0.1 MeV, respectively. Angular distributions were then calculated for each value of J and T using the appropriate expressions in Ref. [12], with the effective moments of inertia obtained as described in the previous subsection. The total angular distribution was obtained by taking the sum of the angular distributions for all values of J and T, weighted by the number of fission events in each bin. The anisotropy was evaluated at the energies shown by the stars in Fig. 8(a), points which correspond to the experimental pre-scission neutron multiplicity data. The uncertainties shown for the calculated points arise from the uncertainties in the measured pre-scission neutron multiplicities and also from the statistical nature of the calculations. These calculations are in good agreement with the experimental anisotropies at all energies. The TSM calculations do not extend below $E_{\rm c.m.} = 71.5$ MeV because the pre-scission neutron multiplicity was not determined below this energy. This result resolves the previous disagreement of the calculated and measured anisotropies for energies below the average fusion barrier. Discrepancies are now at a level which is less than or of the order of the uncertainty in the inputs to the transition state model calculation.

The good agreement of the data with this TSM calculation of the fission fragment angular distributions, in comparison with the previous disagreement, can be attributed to three factors. First, the new experimental anisotropies of this work are lower than those previously measured at energies below the average fusion barrier.

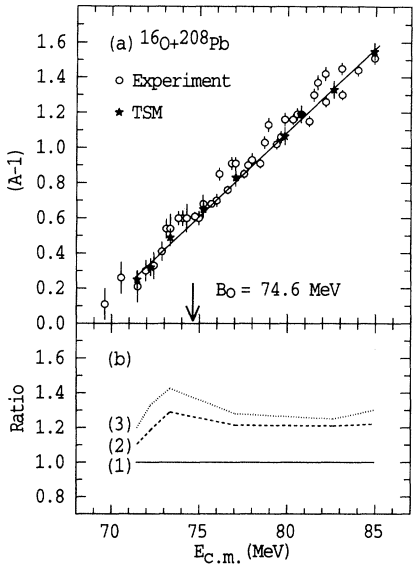

FIG. 8. (a) Comparison between the measured (open circles) and calculated (stars) fission fragment anisotropies for the ^{16}O + ^{208}Pb reaction. The experiment and the calculations are plotted in terms of the reduced anisotropy $(A-1)$. The solid line is a straight line fit to the TSM calculations. (b) The ratio of $(A-1)$ as represented by the solid line in (a) to $(A-1)$ as calculated using different input parameters. A ratio of unity means there is no anomaly, curve (1); a larger ratio means the calculated anisotropies underpredict the experimental anisotropies. The dashed line, curve (2), is the ratio obtained when the anisotropies were calculated using the low values of $\sigma_{\rm ER}$ from Ref. [20]. The effect on curve (2) of using the mean value of the excitation energy instead of the distribution of excitation energies is shown by the dotted line, curve (3).

Secondly, the new ER cross sections are much larger. Finally, there is an effect due to the use of the distribution of saddle-point temperatures in the TSM calculations. These last two factors are discussed below.

The larger values of $\sigma_{\rm ER}$ of this work have two effects on the theoretical anisotropies. Because of the resulting larger fusion cross sections, there is a small increases in the values of $\langle J^2 \rangle$ which increases the calculated anisotropies only slightly. But more importantly, the new larger ER cross sections can only be reproduced in the JOANNE calculations by increasing k_f by a significant amount, while a_f/a_n is changed by a small amount in order to preserve the agreement with the experimental pre-scission neutron multiplicities. These parameters change in this way because the pre-scission neutron multiplicity is very sensitive to a_f/a_n but only weakly dependent on k_f [32]. The overall effect is to significantly reduce the saddle-point temperature, and this has a significant effect on the calculated anisotropies.

In Fig. 8(b), we have attempted to demonstrate the size of these effects, by plotting the ratio of the reduced anisotropy for the best calculation to the reduced

anisotropy of the other calculations. In the following, it is worth emphasizing that there is a complex dependence between each of the parameters in these calculations. Since these calculations were performed with a Monte Carlo code, the curves in Fig. 8(b) have a statistical uncertainty of $\approx 2\%$. The dashed line in Fig. 8(b) is the same as the best calculation, except that the statistical model parameters of JOANNE have been adjusted to fit the smaller values [20] of $\sigma_{\rm ER}$. This calculation also includes the small effects of the different $\langle J^2 \rangle$ values. Above the average barrier, the reduced anisotropies, from the smaller $\sigma_{\rm ER}$, are too low by $\approx 20\%$. The ratio is reasonably constant for the energies above the average barrier, reflecting the fact that the energy dependence of the evaporation residue excitation functions of Ref. [20] and this work [see Fig. 5(b)] are similar. On the basis of Eq. (1), this ratio can be interpreted as the ratio of the T extracted by fitting the larger ER cross section, to the T from the smaller values of $\sigma_{\rm ER}$. Indeed, this was supported by the observation that the ratios of the mean saddle-point temperatures from these two calculations had a very similar magnitude and energy dependence to the ratios of the reduced anisotropies, curve (2) in Fig. 8(b).

Calculating the anisotropy assuming a distribution of excitation energies accounts for some of the increase in the calculations of the theoretical anisotropies. The dotted line in Fig. 8(b) is similar to the TSM calculation of Ref. [13], where the temperature was evaluated assuming a mean value of E^* at the saddle-point and the low values of $\sigma_{\rm ER}$ from Ref. [20]. This has a $\approx 10\%$ effect on the reduced anisotropies.

V. CONCLUSION

Fission and evaporation residue cross sections and fission fragment angular distributions for the reaction ^{16}O + ^{208}Pb were measured in detail at energies around the fusion barrier. The experimental anisotropies have been compared with theoretical values obtained from improved transition state model calculations. The data and the calculations are in agreement, even at energies below the average fusion barrier. Thus, there is no evidence in this reaction of any near-barrier phenomena affecting the fission fragment anisotropies. It has been shown that these comprehensive experimental anisotropies and the more accurate inputs to the transition state model calculations contribute incrementally to this agreement. In particular, reproducing the correct evaporation residue survival probability has a significant effect on the calculated fission fragment anisotropies. There is no longer an anomaly in the fission fragment anisotropies for the ^{16}O + ^{208}Pb reaction, since they can be described by standard models of fusion and fission. This has implications for the interpretation of fission fragment anisotropies in other reactions, since the deviations of the measured anisotropies from those predicted by the standard model can be more reliably used as an indicator of the presence or absence of quasifission.

[1] R. Vandenbosch and J.R. Huizenga, *Nuclear Fission* (Academic Press, New York, 1973).

[2] R. Vandenbosch, Annu. Rev. Nucl. Part. Sci. **42,** 447 (1992).

[3] D.E. Di Gregorio and R.G. Stokstad, Phys. Rev. C **43,** 265 (1991).

[4] A. Charlop, J. Bierman, Z. Drebi, A. García, D. Prindle, A.A. Sonzogni, R. Vandenbosch, D. Ye, S. Gil, F. Hasenbalg, J.E. Testoni, D. Abriola, M. di Tada, A. Etchegoyen, M.C. Berisso, J.O. Fernández-Niello, and A.J. Pacheco, Phys. Rev. C **49,** R1235 (1994).

[5] D. Ackermann, L. Corradi, D.R. Napoli, C.M. Petrache, P. Spolaore, A.M. Stefanini, F. Scarlassara, S. Beghini, G. Montagnoli, G.F. Segato, and C. Signorini, Nucl. Phys. **A575,** 374 (1994).

[6] R. Vandenbosch, T. Murakami, C.-C. Sahm, D.D. Leach, A. Ray, and M.J. Murphy, Phys. Rev. Lett. **56,** 1234 (1986).

[7] J.P. Lestone, J.R. Leigh, J.O. Newton, and J.X. Wei, Nucl. Phys. **A509,** 178 (1990).

[8] B.B. Back, Phys. Rev. C **31,** 2104 (1985).

[9] T. Murakami, C.-C. Sahm, R. Vandenbosch, D.D. Leach, A. Ray, and M.J. Murphy, Phys. Rev. C **34,** 1353 (1986).

[10] Z.H. Lui, H.Q. Zhang, J.C. Xu, X. Qian, Y. Qiao, C.J. Lin, and K. Xu, Phys. Rev. C **50,** 1717 (1994).

[11] J. Tōke, R. Bock, G.X. Dai, A. Gobbi, S. Gralla, K.D. Hildenbrand, J. Kuzminski, W.F.J. Müller, A. Olmi, H. Stelzer, B.B. Back, and S. Bjørnholm, Nucl. Phys. **A440,** 327 (1985).

[12] B.B. Back, R.R. Betts, J.E. Gindler, B.D. Wilkins, S. Saini, M.B. Tsang, C.K. Gelbke, W.G. Lynch, M.A. McMahan, and P.A. Baisden, Phys. Rev. C **32,** 195 (1985).

[13] H. Rossner, D.J. Hinde, J.R. Leigh, J.P. Lestone, J.O. Newton, J.X. Wei, and S. Elfström, Phys. Rev. C **45,** 719 (1992).

[14] D.J. Hinde, M. Dasgupta, J.R. Leigh, J.P. Lestone, J.C. Mein, C.R. Morton, J.O. Newton, and H. Timmers, Phys. Rev. Lett. **74,** 1295 (1995).

[15] W. Reisdorf, F.P. Hessberger, K.D. Hildenbrand, S. Hofmann, G. Münzenberger, K.-H. Schmidt, J.H.R. Schneider, W.F.W. Schneider, K. Sümmerer, G. Wirth, J.V. Kratz, and K. Schlitt, Nucl. Phys. **A438,** 212 (1985); C.H. Dasso, H. Esbensen, and S. Landowne, Phys. Rev. Lett. **57,** 1498 (1986); A.B. Balantekin and P.E. Reimer, Phys. Rev. C **33,** 379 (1986).

[16] J.X. Wei, J.R. Leigh, D.J. Hinde, J.O. Newton, R.C. Lemmon, S. Elfström, and J.X. Chen, Phys. Rev. Lett. **67,** 3368 (1991).

[17] R.C. Lemmon, J.R. Leigh, J.X. Wei, C.R. Morton, D.J. Hinde, J.O. Newton, J.C. Mein, and M. Dasgupta, Phys. Lett. B **316,** 32 (1993).

[18] C.R. Morton, M. Dasgupta, D.J. Hinde, J.R. Leigh, R.C. Lemmon, J.P. Lestone, J.C. Mein, J.O. Newton, H. Timmers, N. Rowley, and A.T. Kruppa, Phys. Rev. Lett. **72,** 4074 (1994).

[19] N. Rowley, J.R. Leigh, J.X. Wei, and R. Lindsay, Phys. Lett. B **314,** 179 (1993).
[20] E. Vulgaris, L. Grodzins, S.G. Steadman, and R. Ledoux, Phys. Rev. C **33,** 2017 (1986).
[21] K. Hartel, Ph.D. thesis, Technical University of Munich, 1985 (unpublished).
[22] K.-T. Brinkmann, A.L. Caraley, B.J. Fineman, N. Gan, J. Velkovska, and R.L. McGrath, Phys. Rev. C **50,** 309 (1994).
[23] V.E. Viola, K. Kwiatkowski, and M. Walker, Phys. Rev. C **31,** 1550 (1985).
[24] D.F. Torgerson and R.D. Macfarlane, Nucl. Phys. **A149,** 641 (1970); K. Valli, E.K. Hyde, and J. Borggreen, Phys. Rev. C **1,** 2115 (1970); O. Häusser, W. Witthuhn, T.K. Alexander, A.B. McDonald, J.C.D. Milton, and A. Olin, Phys. Rev. Lett. **31,** 323 (1973).
[25] F. Videbæk, R.B. Goldstein, L. Grodzins, and S.G. Steadman, Phys. Rev. C **15,** 954 (1977).
[26] N. Rowley, G.R. Satchler, and P.H. Stelson, Phys. Lett. B **254,** 25 (1991).
[27] J.P. Lestone, Phys. Rev. C **51,** 580 (1995).
[28] P. Fröbrich and H. Rossner, Z. Phys. A **349,** 99 (1994).
[29] J.P. Lestone, J.R. Leigh, J.O. Newton, D.J. Hinde, J.X. Wei, J.X. Chen, S. Elfström, and M. Zielinska-Pfabé, Nucl. Phys. **A559,** 277 (1993).
[30] A.J. Sierk, Phys. Rev. C **33,** 2039 (1986).
[31] H.A. Weidenmüller and Z. Jing-Shang, Phys. Rev. C **29,** 879 (1984).
[32] D. Ward, R.J. Charity, D.J. Hinde, J.R. Leigh, and J.O. Newton, Nucl. Phys. **A403,** 189 (1983).